A New Magnetic Parameter of Active Regions Distinguishing Large Eruptive and Confined Solar Flares

Ting Li[1,2] ⓘ, Xudong Sun[3] ⓘ, Yijun Hou[1,2] ⓘ, Anqin Chen[4] ⓘ, Shuhong Yang[1,2] ⓘ, and Jun Zhang[5]
[1] CAS Key Laboratory of Solar Activity, National Astronomical Observatories, Chinese Academy of Sciences, Beijing 100101, People's Republic of China
liting@nao.cas.cn
[2] School of Astronomy and Space Science, University of Chinese Academy of Sciences, Beijing 100049, People's Republic of China
[3] Institute for Astronomy, University of Hawai'i at Mānoa, Pukalani, HI 96768, USA
[4] Key Laboratory of Space Weather, National Center for Space Weather, China Meteorological Administration, Beijing 100081, People's Republic of China
[5] School of Physics and Optoelectronics engineering, Anhui University, Hefei 230601, People's Republic of China

Abstract

With the aim of investigating how the magnetic field in solar active regions (ARs) controls flare activity, i.e., whether a confined or eruptive flare occurs, we analyze 106 flares of Geostationary Operational Environmental Satellite class $\geqslant$M1.0 during 2010–2019. We calculate mean characteristic twist parameters α_{FPIL} within the "flaring polarity inversion line" region and α_{HFED} within the area of high photospheric magnetic free energy density, which both provide measures of the nonpotentiality of the AR core region. Magnetic twist is thought to be related to the driving force of electric current-driven instabilities, such as the helical kink instability. We also calculate total unsigned magnetic flux (Φ_{AR}) of ARs producing the flare, which describes the strength of the background field confinement. By considering both the constraining effect of background magnetic fields and the magnetic nonpotentiality of ARs, we propose a new parameter $\alpha/\Phi_{\mathrm{AR}}$ to measure the probability for a large flare to be associated with a coronal mass ejection (CME). We find that in about 90% of eruptive flares, $\alpha_{\mathrm{FPIL}}/\Phi_{\mathrm{AR}}$ and $\alpha_{\mathrm{HFED}}/\Phi_{\mathrm{AR}}$ are beyond critical values (2.2×10^{-24} and 3.2×10^{-24} Mm^{-1} Mx^{-1}), whereas they are less than critical values in ~80% of confined flares. This indicates that the new parameter $\alpha/\Phi_{\mathrm{AR}}$ is well able to distinguish eruptive flares from confined flares. Our investigation suggests that the relative measure of magnetic nonpotentiality within the AR core over the restriction of the background field largely controls the capability of ARs to produce eruptive flares.

Unified Astronomy Thesaurus concepts: Solar activity (1475); Solar active region magnetic fields (1975); Solar flares (1496); Solar coronal mass ejections (310)

1. Introduction

Solar flares and coronal mass ejections (CMEs) are the rapid release of a huge amount of magnetic energy accumulated in the solar corona through magnetohydrodynamic instabilities and magnetic reconnection. Solar flares are often, but not always, accompanied by CMEs. We refer to flares with a CME as "eruptive flares" and flares not associated with a CME as "confined flares." It is revealed that flare–CME association rate increases with the flare intensity (Andrews 2003; Yashiro et al. 2006). Recently, Li et al. (2020, 2021) found that flare–CME association rate decreases with total unsigned magnetic flux (Φ_{AR}) of active regions (ARs) producing the flare, which provides a global parameter relating to the strength of the background field confinement.

Over the past two decades, significant progress has been made in understanding the physical factors determining whether a flare event is associated with a CME or not. It is suggested that eruptive flares tend to occur if the overlying background magnetic fields are weaker or more quickly decay with height (Török & Kliem 2005; Wang & Zhang 2007; Wang et al. 2017; Amari et al. 2018; Baumgartner et al. 2018; Jing et al. 2018; Duan et al. 2019). Moreover, the magnetic nonpotentiality of ARs is thought to be another important factor governing the eruptive character of solar

flares (Nindos & Andrews 2004; Liu et al. 2016; Cui et al. 2018; Vasantharaju et al. 2018; Thalmann et al. 2019; Avallone & Sun 2020; Gupta et al. 2021), such as free magnetic energy, relative helicity, magnetic twists, etc. Statistical studies have shown that CME productivity is correlated with the twist parameter α (Falconer et al. 2002, 2006), which characterizes the degree to which the photospheric magnetic fields of an AR deviate from a potential field (Leka & Skumanich 1999; Yang et al. 2012). Bobra & Ilonidis (2016) found that the twist parameter α and mean gradient of the horizontal field are two relatively high-performing features in predicting CMEs based on machine-learning algorithms. However, the measurement of previous known parameters showed that there are high degrees of overlap between confined and eruptive flares if only one factor (overlying confinement or magnetic nonpotentiality) was considered in selecting the parameters (Nindos & Andrews 2004; Wang et al. 2017; Vasantharaju et al. 2018).

Sun et al. (2015) suggested that AR eruptivity is related to the relative value of magnetic nonpotentiality over the restriction of the background field. In this Letter, following the idea of Sun et al. (2015), we consider both the constraining effect of background magnetic fields and the magnetic nonpotentiality of ARs, and propose a new parameter $\alpha/\Phi_{\mathrm{AR}}$ to describe the eruptive character of a flare. By measuring the parameter of 106 large flares within the cores of 12 CME-active and 9 CME-quiet ARs, we find that the new parameter $\alpha/\Phi_{\mathrm{AR}}$ is well able to distinguish flares associated with CMEs from flares that are not.

2. Database Selection and Parameter Calculations

We use a subset of 106 flare events[6] $\geqslant$M1.0 (43 eruptive and 63 confined) from a large database of 322 M-class flares[7] during the period of 2010 June–2019 June (Li et al. 2020). The subset is selected based on the characteristics of ARs, and the selected ARs must fulfill the following two selection criteria. First, the ARs are flare-active and produced $\geqslant$ 3 M-class flares. Second, the ARs can be unambiguously classified into CME-active and CME-quiet ARs. We refer to an AR as a CME-active (CME-quiet) AR if the flares from it are all eruptive (confined) or only one exceptional flare is confined (eruptive). Finally, a total of 21 ARs fulfill these selection criteria, including 12 CME-active ARs and 9 CME-quiet ARs.

For each event, based on the vector magnetograms from Space-Weather Helioseismic and Magnetic Imager (HMI; Scherrer et al. 2012) AR Patches (SHARP; Bobra et al. 2014) observed by Solar Dynamics Observatory (SDO; Pesnell et al. 2012), we calculate Φ_{AR} before the flare onset by summing all pixels where vertical magnetic field $|B_z| > 100$ G (Kazachenko et al. 2017). The magnetograms are remapped using a cylindrical equal area (CEA) projection with a pixel size of $\sim 0\rlap{.}''5$ and presented as (B_r, B_θ, B_ϕ) in heliocentric spherical coordinates corresponding to $(B_z, -B_y, B_x)$ in heliographic coordinates (Sun 2013). We have identified a flaring polarity inversion line (FPIL) mask to demarcate the core of an AR by using the method of Sun et al. (2015). We first find the polarity inversion line (PIL) pixels from a smoothed vertical magnetic field B_z, and dilate them with a circular kernel with a radius of 18 pixels (about 6.5 Mm; other radii are also used and the results are not affected). Then we isolate flare ribbons by using the 1600 Å image near the flare peak from the Atmospheric Imaging Assembly (AIA; Lemen et al. 2012) on board the SDO (above 700 DN s^{-1}, which is about 10 times the standard deviation above the mean of the quiet-Sun values), and dilate them with a large kernel having a radius of 20 pixels (about 7.2 Mm). Finally the intersection of dilated PIL and ribbon areas is considered to be the FPIL mask. The FPIL mask is similar to the strong-field, high-gradient PIL mask in Schrijver (2007); however, it only involves part of the PIL mask.

We calculate distributions of vertical electric current density J_z and the mean characteristic twist parameter α_{FPIL} within the FPIL mask region. We note that the FPIL mask region could be determined only after the flare occurrence and thus α_{FPIL} cannot be used for CME forecasting. The energy release during a flare is generally believed to originate from areas with high values of photospheric magnetic free energy density ρ_{free} in ARs, and thus we select the region with $\rho_{free} > 4.0 \times 10^4$ erg cm^{-3} (HFED region; Chen & Wang 2012) as a proxy for the AR core region and calculate mean characteristic twist parameter α_{HFED} and mean shear angle Ψ_{HFED} within the HFED region. Compared with α_{FPIL}, α_{HFED} does not need ribbon information and is more suitable for CME forecasting. Detailed formulas of the parameters are listed in Table 1.

3. Statistical Results

Figure 1 shows four examples of two eruptive and two confined flares, which includes 1600 Å images (left),

Table 1
Parameters Used to Distinguish the Eruptive and Confined Flares[a]

| Parameters	Description	Unit	Formula
Φ_{AR}	Total unsigned flux	Mx	$\Phi_{AR} = \Sigma|B_z|dA$
J_z	Mean vertical electric current density	mA m^{-2}	$J_z = \frac{1}{N\mu}\Sigma(\nabla \times \mathbf{B})_z$[b]
α	Mean characteristic twist parameter	Mm^{-1}	$\alpha = \frac{\mu\Sigma J_z B_z}{\Sigma B_z^2}$
ρ_{free}	Magnetic free energy density	erg cm^{-3}	$\rho_{free} = \frac{1}{8\pi}|\mathbf{B}_{obs}-\mathbf{B}_{pot}|^2$
Ψ	Mean shear angle	degree	$\Psi = \arccos\frac{\mathbf{B}_{obs}\cdot\mathbf{B}_{pot}}{|B_{obs}B_{pot}|}$

Notes.
[a] Adapted from Chen & Wang (2012) and Bobra et al. (2014).
[b] μ is the magnetic permeability in vacuum ($4\pi \times 10^{-3}$ G m A^{-1}).

photospheric magnetograms (middle), and derived vertical electric current density J_z maps (right). We can see that for two eruptive flares (X2.1 flare in AR 11283 and M6.5 in AR 12371) the positive and negative currents have a coherent structure around the PIL (Figures 1(a)–(b)), indicating the presence of "current ribbons" as in a coherent flux rope. However, the two confined events (X3.1 in AR 12192 and M6.1 in AR 12222) exhibit disordered current distributions and do not have any noticeable structure (Figures 1(c)–(d)). It also can been seen that the FPIL mask regions (orange and black contours) overlap the area of large currents, implying that the FPIL mask corresponds to the AR core with the strongest magnetic nonpotentiality. We estimate the errors of J_z to be about 10 mA m^{-2} based on the noise level of transverse magnetic field ($\sim$100 G in Liu et al. 2012).

Based on the derived J_z map, we then calculated the mean characteristic twist parameter α_{FPIL} within the FPIL mask region for the 106 flares. Figure 2(a) shows the scatterplot of α_{FPIL} versus Φ_{AR}. Blue (red) circles are the eruptive (confined) flares. It needs to be noted that α_{FPIL} is a signed parameter and in our study α_{FPIL} means its absolute value. It can be seen that the events with $\alpha_{FPIL} < 0.07$ Mm^{-1} (black dotted line in Figure 2(a)) and $\Phi_{AR} > 1.0 \times 10^{23}$ Mx (right green dashed line in Figure 2(a)) are all confined and those with $\alpha_{FPIL} \geqslant 0.07$ Mm^{-1} and $\Phi_{AR} < 3.5 \times 10^{22}$ Mx (left green dashed line in Figure 2(a)) are all eruptive. According to error propagation theory, we estimate the errors of α_{FPIL} to be 10^{-4}–10^{-3} Mm^{-1} (by considering the error of $J_z \sim 10$ mA m^{-2}). The errors are small and they do not affect our results. The noise level of B_z is on the order of 10 G (Liu et al. 2012), and the errors in the calculation of Φ_{AR} are estimated to be about 10^{18}–10^{19} Mx. The errors are much smaller than Φ_{AR} and thus are not considered. Figure 2(b) shows the scatterplot of flare peak X-ray flux versus α_{FPIL}/Φ_{AR}. About 93% (40 of 43) of eruptive events have $\alpha_{FPIL}/\Phi_{AR} \geqslant 2.2 \times 10^{-24}$ Mm^{-1} Mx^{-1}, and $\sim$83% (52 of 63) of confined flares have $\alpha_{FPIL}/\Phi_{AR} < 2.2 \times 10^{-24}$ Mm^{-1} Mx^{-1} (black dashed–dotted line in Figure 2(b)). This shows that the new relative nonpotential parameter α_{FPIL}/Φ_{AR} is well able to distinguish the two populations of eruptive and confined flares. The statistical comparison between the two distributions in Figure 2(b) was done with a two-sample t-test, which shows a significant difference (P < 0.001). However, there is still a small overlap (14 of 106) by using our criterion and the exceptional events
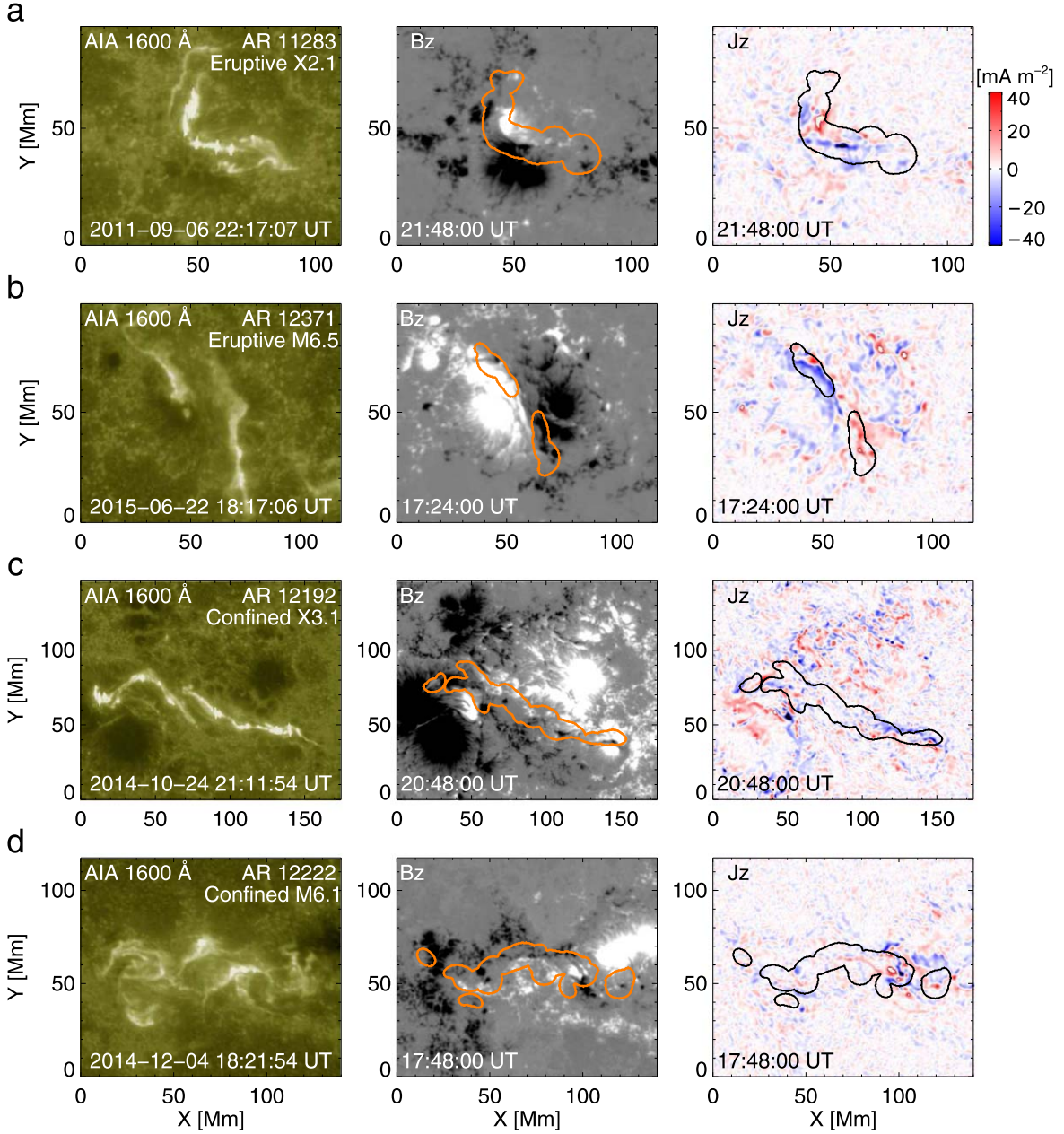

Figure 1. Four examples of two eruptive and two confined flares showing SDO/AIA 1600 Å images (left), SDO/HMI photospheric magnetograms B_z (middle), and derived vertical electric current density J_z maps (right). From top to bottom: eruptive X2.1-class flare in AR 11283, eruptive M6.5-class flare in AR 12371, confined X3.1-class flare in AR 12192, and confined M6.1-class flare in AR 12222. AIA 1600 Å images were remapped with CEA projection. Orange and black contours outline the FPIL mask regions within which the mean characteristic twist parameter (α_{FPIL}) in Figure 2 was calculated.

are mainly from a CME-active AR 11302 and two CME-quiet ARs 11476 and 12268.

Figure 3 shows the maps of photospheric magnetic free energy density ρ_{free} and magnetic shear angle Ψ for the four examples shown in Figure 1. Free magnetic energy is the amount of magnetic energy in excess of the minimum energy attributed to the potential field, and magnetic shear is defined as the angle between the horizontal components of the observed magnetic field and a modeled potential magnetic field based on photospheric B_z map. They are commonly used parameters in describing the magnetic complexity and nonpotentiality (Wang et al. 1994; Su et al. 2014). It can be seen that the maps of ρ_{free} and Ψ exhibit similar distributions, with their large values around the PILs of ARs. The comparison of two eruptive flares

(Figures 3(a)–(b)) with two confined ones (Figures 3(c)–(d)) shows that the mean values of ρ_{free} and Ψ of eruptive flares are larger than those of confined events. Similar to the appearance of J_z maps (Figure 1), ρ_{free} and Ψ of eruptive flares exhibit ribbon patterns; however, the ρ_{free} and Ψ maps of confined flares show disordered distributions.

We determine high-ρ_{free} areas (HFED region) as a proxy for the AR core region and then calculate mean characteristic twist parameter α_{HFED} and mean shear angle Ψ_{HFED} within the HFED region. Figure 4 shows the calculation results for 43 eruptive and 63 confined flares. It can be seen that the distributions of α_{HFED} (Figure 4(a)) are similar to those of α_{FPIL} (Figure 2(a)). For $\alpha_{\mathrm{HFED}} < 0.1$ Mm^{-1} (black dotted line in Figure 4(a)), an overwhelming majority (about 93%, 26 out
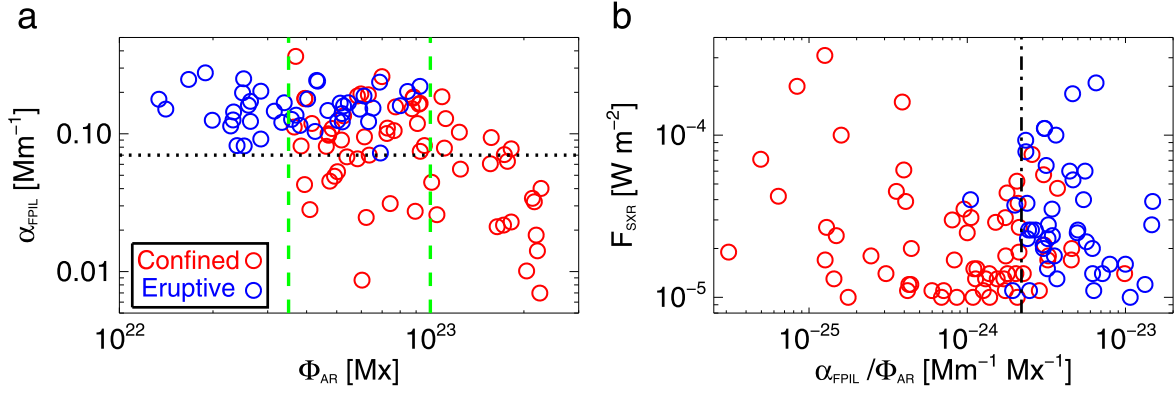
Figure 2. Scatterplots of mean characteristic twist parameter α_{FPIL} vs. total unsigned magnetic flux Φ_{AR} and flare peak X-ray flux F_{SXR} vs. α_{FPIL}/Φ_{AR}. Blue (red) circles are eruptive (confined) flares. Two vertical green lines in panel (a) correspond to Φ_{AR} of 3.5×10^{22} Mx and 1.0×10^{23} Mx, respectively. The horizontal black line in panel (a) refers to α_{FPIL} of 0.07 Mm^{-1}. The vertical black line in panel (b) denotes α_{FPIL}/Φ_{AR} of 2.2×10^{-24} Mm^{-1} Mx^{-1}.

of 28) of flares are confined. Almost all the eruptive flares (41 out of 43) have $\alpha_{HFED} \geqslant 0.1$ Mm^{-1}. If we consider the relative parameter α_{HFED}/Φ_{AR}, the differences between confined and eruptive cases are more evident (Figure 4(b)). About 91% (39 of 43) of eruptive flares have $\alpha_{HFED}/\Phi_{AR} \geqslant 3.2 \times 10^{-24}$ Mm^{-1} Mx^{-1}, and ~75% (47 of 63) of confined events have $\alpha_{HFED}/\Phi_{AR} < 3.2 \times 10^{-24}$ Mm^{-1} Mx^{-1} (black dashed–dotted line in Figure 4(b)). There is also a difference of mean shear angle Ψ_{HFED} within the HFED region between eruptive and confined flares (Figure 4(c)). The proportion of confined flares is ~91% (29 of 32) corresponding to $\Psi_{HFED} < 60°$. Similarly, the relative parameter Ψ_{HFED}/Φ_{AR} can provide a good ability for distinguishing the eruptive and confined events (Figure 4(d)). An overwhelming majority of eruptive flares have $\Psi_{HFED}/\Phi_{AR} \geqslant 1°.0 \times 10^{-21}$ Mx^{-1} and most of the confined flares show $\Psi_{HFED}/\Phi_{AR} < 1°.0 \times 10^{-21}$ Mx^{-1}. The degree of overlap between eruptive and confined events for Ψ_{HFED}/Φ_{AR} is a little higher than that for α_{HFED}/Φ_{AR}. The two-sample t-test was carried out for the two parameters in Figures 4(b) and (d), and showed a significant difference (P < 0.001).

4. Summary and Discussion

In this study, we have analyzed the magnetic nonpotentiality of ARs and the constraining effect of background fields for 106 flares $\geqslant$M1.0-class from 12 CME-active and 9 CME-quiet ARs. We proposed a new parameter α_{FPIL}/Φ_{AR} that is well able to distinguish ARs with the capability of producing eruptive flares. About 93% of eruptive events have the distributions of $\alpha_{FPIL}/\Phi_{AR} \geqslant 2.2 \times 10^{-24}$ Mm^{-1} Mx^{-1}, and ~83% of confined flares have $\alpha_{FPIL}/\Phi_{AR} < 2.2 \times 10^{-24}$ Mm^{-1} Mx^{-1}. Moreover, we select the areas of high photospheric magnetic free energy density before the flare onset as a proxy for the AR core region to calculate mean characteristic twist parameter α_{HFED} and mean shear angle Ψ_{HFED}. The statistical results showed that the relative parameters α_{HFED}/Φ_{AR} and Ψ_{HFED}/Φ_{AR} can also provide a good ability for distinguishing the eruptive and confined flares. Overall, about 81% (86 out of 106) of flare events can be classified into the two populations of confined and eruptive flares using the parameter α_{HFED}/Φ_{AR} (through determining a critical value). The performance of Ψ_{HFED}/Φ_{AR} is not as good as that of α_{HFED}/Φ_{AR}, and about 74% (78 out of 106) of flare events can be distinguished.

Parameter α is the average characteristic twist of the magnetic field lines around the PILs of an AR, and provide

measures of the nonpotentiality of the AR core region (Leka & Skumanich 1999; Benson et al. 2021). Previous studies have shown that the parameter of magnetic twist plays an important role in discriminating between confined and eruptive events and can be used to predict whether an X- or M-class flaring AR would produce a CME (Bobra & Ilonidis 2016; Duan et al. 2019). Magnetic twist is thought to be related to the driving force of electric current-driven instabilities, such as the helical kink instability (Hood & Priest 1979). An AR containing a highly twisted magnetic field tends to produce an eruption when the twist exceeds a certain threshold. On the other hand, according to the study of Li et al. (2020), Φ_{AR} has a high positive correlation with the critical decay index height (related to the torus instability of a magnetic flux rope; Kliem & Török 2006), implying that Φ_{AR} describes the strength of the background field confinement. Our statistical study reveals that the relative parameter α/Φ_{AR} has a better performance in distinguishing between the two types of flares than only Φ_{AR} or α does. We suggest that the relative parameter α/Φ_{AR} indicates the balance between the upward force that drives the eruptions and the downward force that suppresses the eruptions.

Recently, several studies have shown the general trend that confined events have a smaller reconnection flux fraction (Φ_{ribbon}/Φ_{AR}; defined by the ratio between the flux swept by the flare ribbons to the total AR flux) compared with eruptive flares (Toriumi et al. 2017; Li et al. 2020; Kazachenko et al. 2021). However, there is a considerable overlap between the flux fraction distributions of confined and eruptive flares. Comparably, our parameters α/Φ_{AR} and α_{HFED}/Φ_{AR} show more significant differences in distributions between the two populations of flares. We hypothesize that Φ_{ribbon} involves part of overlying background confining fields of ARs participating in the flare reconnection at the late stage of the flare. In comparison, α_{FPIL} and α_{HFED} only correspond to the preflare high-twist fields in an AR core region, which are strongly related to the initial driving force of solar flares. Therefore, α_{FPIL}/Φ_{AR} and α_{HFED}/Φ_{AR} can provide a better ability to distinguish the eruptive and confined events than Φ_{ribbon}/Φ_{AR}.

The idea of the new parameter α/Φ_{AR} can be generalized to "relative nonpotentiality," which refers to the ratio of magnetic flux (or other physical quantities) in a flux rope to that in the surrounding magnetic structures (Lin et al. 2021). A larger relative nonpotentiality indicates a higher probability for a flux rope to erupt (Toriumi et al. 2017; Thalmann et al. 2019; Gupta et al. 2021). Recently, Lin et al. (2020) proposed a new relative
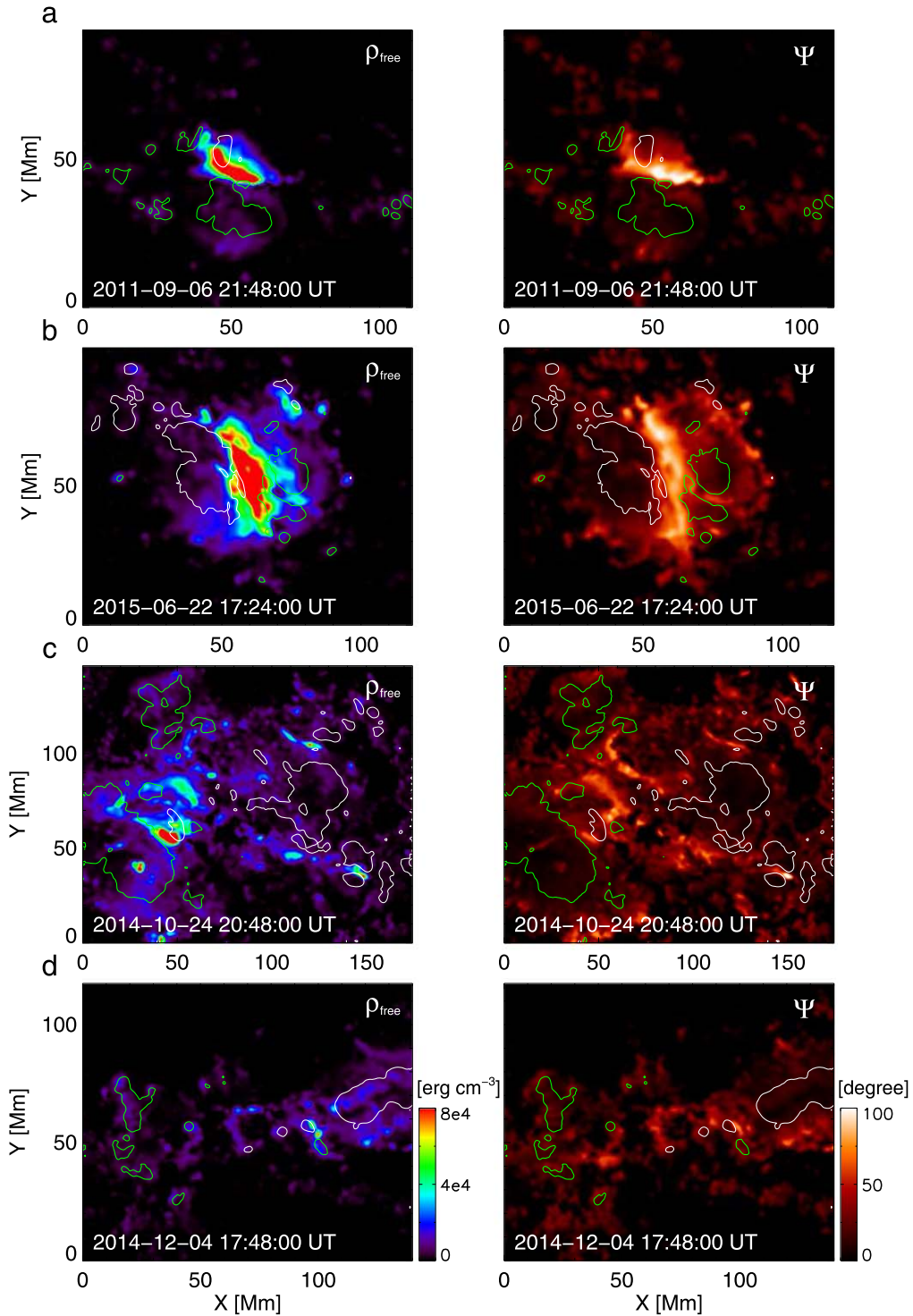
Figure 3. Maps of photospheric free magnetic energy density $\rho_{\rm free}$ and magnetic shear angle Ψ of four examples (from top to bottom: eruptive X2.1-class flare in AR 11283, eruptive M6.5-class flare in AR 12371, confined X3.1-class flare in AR 12192, and confined M6.1-class flare in AR 12222). The white and green contours are the magnetic fields B_z at $\pm$ 800 G levels. Mean characteristic twist parameter $\alpha_{\rm HFED}$ and mean shear angle $\Psi_{\rm HFED}$ in Figure 4 are calculated within the areas of $\rho_{\rm free} > 4.0 \times 10^4$ erg cm^{-3}.

nonpotentiality parameter of the magnetic flux in the highly twisted region relative to its ambient background fields, which demonstrated a moderate ability in discriminating between confined and ejective events. It seems that our parameters $\alpha/\Phi_{\rm AR}$ show a better classification performance than the parameter proposed in Lin et al. (2020). For instance, two events of X1.6- and X3.1-class flares in AR 12192 failed to be

correctly classified in Lin et al. (2020, 2021); however, they can be correctly classified in our study. However, due to the difference of selected samples, a direct comparison cannot be carried out.

In recent years, the importance of the confinement of flux ropes by overlying loops (and thus the importance of structural relativity) has been actively discussed in the theoretical and
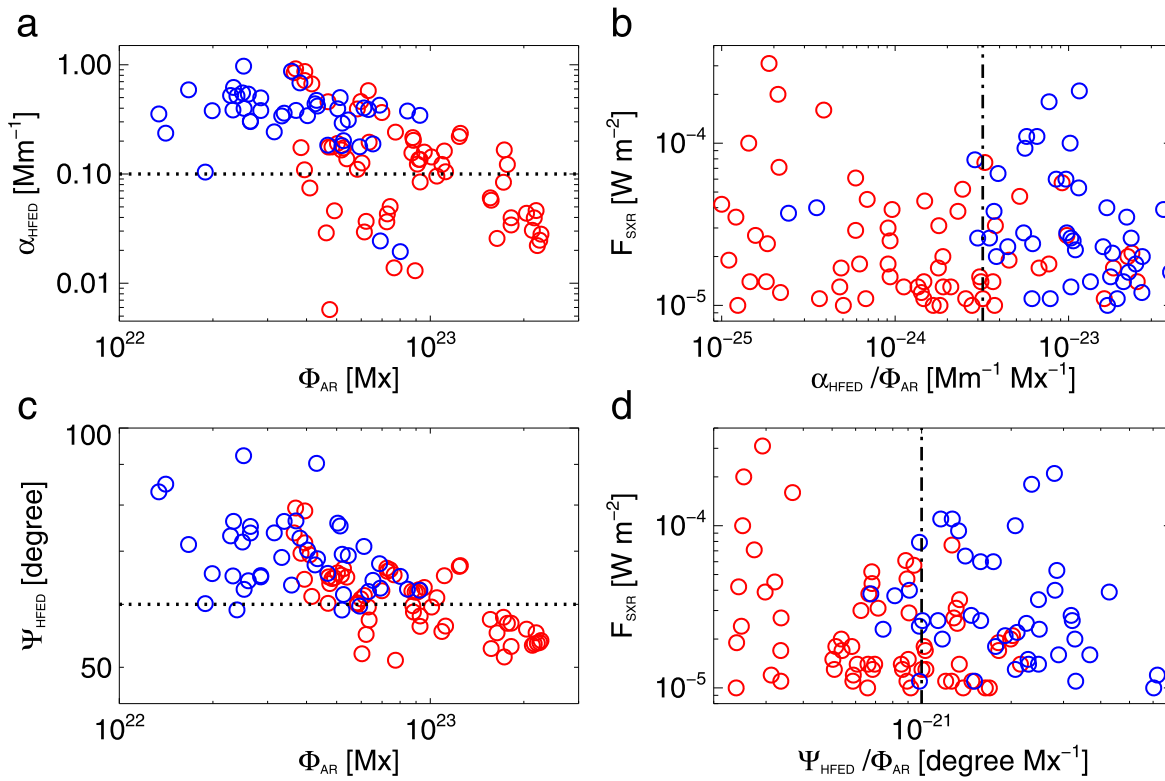
Figure 4. Similar to Figure 2, but for mean characteristic twist parameter α_{HFED} and mean shear angle Ψ_{HFED} within the HFED region. Blue (red) circles are eruptive (confined) flares. The horizontal dotted line in panel (a) corresponds to α_{HFED} of 0.1 Mm^{-1}. The vertical dashed–dotted line in panel (b) refers to α_{HFED}/Φ_{AR} of 3.2×10^{-24} Mm^{-1} Mx^{-1}. The horizontal dotted line in panel (c) denotes Ψ_{HFED} of 60°. The vertical dashed–dotted line in panel (d) corresponds to Ψ_{HFED}/Φ_{AR} of $1°.0 \times 10^{-21}$ Mx^{-1}.

modeling studies. Leake et al. (2013) simulated a magnetic flux emergence into preexisting dipole coronal field and found that it becomes a stable flux rope if the dipole coronal field is oriented to minimize magnetic reconnection. Using the same simulation results, Pariat et al. (2017) found that the ratio of the magnetic helicity of the current-carrying magnetic field to the total relative helicity diagnoses very clearly the eruptive potential of their parametric simulations. Toriumi & Takasao (2017) conducted flux emergence models and showed that the confinement of the flux rope or the access to the outer space depends on the large-scale AR structures, which determines the CME eruption. The CME eruption is predicted by the SHARP parameters that characterize the "relativity" between the flaring zone and overall AR area. Amari et al. (2018) suggested that the role of the magnetic cage is one deciding factor for the success or failure of CMEs.

Our findings imply that the relative measure of magnetic nonpotentiality within the AR core over the restriction of the background field largely controls whether a flare is eruptive or confined. However, it needs to be noted that there is still a small overlap (less than 20%) between the two populations of confined and eruptive flares by using parameter α/Φ_{AR}. We suggest that other unknown mechanisms or intrinsic stochasticity may also play a role in governing CME production.

ORCID iDs

Ting Li ⓘ https://orcid.org/0000-0001-6655-1743
Xudong Sun ⓘ https://orcid.org/0000-0003-4043-616X
Yijun Hou ⓘ https://orcid.org/0000-0002-9534-1638
Anqin Chen ⓘ https://orcid.org/0000-0002-3325-7385
Shuhong Yang ⓘ https://orcid.org/0000-0002-6565-3251

References

Amari, T., Canou, A., Aly, J.-J., et al. 2018, Natur, 554, 211
Andrews, M. D. 2003, SoPh, 218, 261
Avallone, E. A., & Sun, X. 2020, ApJ, 893, 123
Baumgartner, C., Thalmann, J. K., & Veronig, A. M. 2018, ApJ, 853, 105
Benson, B., Pan, W. D., Prasad, A., et al. 2021, SoPh, 296, 163
Bobra, M. G., & Ilonidis, S. 2016, ApJ, 821, 127
Bobra, M. G., Sun, X., Hoeksema, J. T., et al. 2014, SoPh, 289, 3549
Chen, A. Q., & Wang, J. X. 2012, A&A, 543, A49
Cui, Y., Wang, H., Xu, Y., et al. 2018, JGRA, 123, 1704
Duan, A., Jiang, C., He, W., et al. 2019, ApJ, 884, 73
Falconer, D. A., Moore, R. L., & Gary, G. A. 2002, ApJ, 569, 1016
Falconer, D. A., Moore, R. L., & Gary, G. A. 2006, ApJ, 644, 1258
Gupta, M., Thalmann, J. K., & Veronig, A. M. 2021, A&A, 653, A69
Hood, A. W., & Priest, E. R. 1979, SoPh, 64, 303

Jing, J., Liu, C., Lee, J., et al. 2018, ApJ, 864, 138
Kazachenko, M. D., Lynch, B. J., Savcheva, A., et al. 2021, arXiv:2111.06048
Kazachenko, M. D., Lynch, B. J., Welsch, B. T., et al. 2017, ApJ, 845, 49
Kliem, B., & Török, T. 2006, PhRvL, 96, 255002
Leake, J. E., Linton, M. G., & Török, T. 2013, ApJ, 778, 99
Leka, K. D., & Skumanich, A. 1999, SoPh, 188, 3
Lemen, J. R., Title, A. M., Akin, D. J., et al. 2012, SoPh, 275, 17
Li, T., Chen, A., Hou, Y., et al. 2021, ApJL, 917, L29
Li, T., Hou, Y., Yang, S., et al. 2020, ApJ, 900, 128
Lin, P. H., Kusano, K., & Leka, K. D. 2021, ApJ, 913, 124
Lin, P. H., Kusano, K., Shiota, D., et al. 2020, ApJ, 894, 20
Liu, L., Wang, Y., Wang, J., et al. 2016, ApJ, 826, 119
Liu, Y., Hoeksema, J. T., Scherrer, P. H., et al. 2012, SoPh, 279, 295
Nindos, A., & Andrews, M. D. 2004, ApJL, 616, L175
Pariat, E., Leake, J. E., Valori, G., et al. 2017, A&A, 601, A125
Pesnell, W. D., Thompson, B. J., & Chamberlin, P. C. 2012, SoPh, 275, 3

Scherrer, P. H., Schou, J., Bush, R. I., et al. 2012, SoPh, 275, 207
Schrijver, C. J. 2007, ApJL, 655, L117
Su, J. T., Jing, J., Wang, S., et al. 2014, ApJ, 788, 150
Sun, X. 2013, arXiv:1309.2392
Sun, X., Bobra, M. G., Hoeksema, J. T., et al. 2015, ApJL, 804, L28
Thalmann, J. K., Moraitis, K., Linan, L., et al. 2019, ApJ, 887, 64
Toriumi, S., Schrijver, C. J., Harra, L. K., et al. 2017, ApJ, 834, 56
Toriumi, S., & Takasao, S. 2017, ApJ, 850, 39
Török, T., & Kliem, B. 2005, ApJL, 630, L97
Vasantharaju, N., Vemareddy, P., Ravindra, B., et al. 2018, ApJ, 860, 58
Wang, D., Liu, R., Wang, Y., et al. 2017, ApJL, 843, L9
Wang, H., Ewell, M. W., Zirin, H., et al. 1994, ApJ, 424, 436
Wang, Y., & Zhang, J. 2007, ApJ, 665, 1428
Yang, X., Zhang, H., Gao, Y., et al. 2012, SoPh, 280, 165
Yashiro, S., Akiyama, S., Gopalswamy, N., et al. 2006, ApJL, 650, L143